Published in final edited form as:
J Proteome Res. 2011 November 4; 10(11): 5232–5241. doi:10.1021/pr200800w.

Magic Angle Spinning NMR Based Metabolic Profiling of Head and Neck Squamous Cell Carcinoma Tissues

Bagganahalli S. Somashekar[1,#], **Pachiyappan Kamarajan**[2,#], **Theodora Danciu**[2], **Yvonne L. Kapila**[2], **Arul M. Chinnaiyan**[3,4,5,6], **Thekkelnaycke M. Rajendiran**[3], and **Ayyalusamy Ramamoorthy**[1,*]

[1]Department of Chemistry and Biophysics, University of Michigan, Ann Arbor, MI, USA

[2]Department of Periodontics and Oral Medicine, School of Dentistry, University of Michigan, Ann Arbor, MI, USA

[3]Michigan Center for Translational Pathology, Department of Pathology, University of Michigan Medical School, Ann Arbor, MI, USA

[4]Department of Urology, University of Michigan Medical School, Ann Arbor, MI, USA

[5]Comprehensive Cancer Center, University of Michigan Medical School, Ann Arbor, MI, USA

[6]Howard Hughes Medical Institute, University of Michigan Medical School, Ann Arbor, MI, USA

Abstract

High-resolution magic-angle spinning (HR-MAS) proton NMR spectroscopy is used to explore the metabolic signatures of head and neck squamous cell carcinoma (HNSCC) which included matched normal adjacent tissue (NAT) and tumor originating from tongue, lip, larynx and oral cavity, and associated lymph-node metastatic (LN-Met) tissues. A total of 43 tissues (18 NAT, 18 Tumor and 7 LN-Met) from twenty-two HNSCC patients were analyzed. Principal Component Analysis of NMR data showed a clear classification between NAT and tumor tissues, however, LN-Met tissues were classified among tumor. A partial least squares discriminant analysis model generated from NMR metabolic profiles was used to differentiate normal from tumor samples (Q^2 > 0.80, Receiver Operator Characteristic area under the curve > 0. 86, using 7-fold cross validation). HNSCC and LN-Met tissues showed elevated levels of lactate, amino acids including leucine, isoleucine, valine, alanine, glutamine, glutamate, aspartate, glycine, phenylalanine and tyrosine, choline containing compounds, creatine, taurine, glutathione and decreased levels of triglycerides. These elevated metabolites were associated with highly active glycolysis, increased amino acids influx (anaplerosis) into the TCA cycle, altered energy metabolism, membrane choline phospholipid metabolism, and oxidative and osmotic defense mechanisms. Moreover, decreased levels of triglycerides may indicate lipolysis followed by β-oxidation of fatty acids that may exist to deliver bioenergy for rapid tumor cell proliferation and growth.

Keywords

HR-MAS NMR; Metabolites; Metabolomics; Head and Neck Squamous Cell Carcinoma; Lymph-node metastasis

[*]Corresponding Author, Prof. Ayyalusamy Ramamoorthy, Biophysics and Department of Chemistry, University of Michigan, 930 North University Avenue, Ann Arbor, Michigan 48109-1055, USA, Phone: (734) 647-6572, Fax: (734) 764-3323, ramamoor@umich.edu.
[#]Authors contributed equally.

Supporting Information Available: Supporting Information Available: This material is available free of charge via the Internet at http://pubs.acs.org.

INTRODUCTION

Head and neck squamous cell carcinoma (HNSCC) represents a group of biologically similar cancer originating from various sites of the upper aerodigestive tract including lip, oral cavity, tongue, larynx, nasal cavity, paranasal sinuses and pharynx. Tobacco and alcohol consumption are the most important risk factors for head and neck cancers.[1] HNSCC accounts for approximately 3% of all human malignancies and is the fifth most common form of cancer worldwide.[2] In the United States, the estimated number of newly diagnosed HNSCC cases are 78,800 and 15,800 deaths in 2011.[2] HNSCC is diagnosed based on physical examination, endoscopy, x-ray, computed tomography[2], magnetic resonance imaging, and blood and urine tests. Nevertheless, definitive diagnosis relies on histopathological examination of tissue biopsies, according to the World Health Organization classification of tumors. Management of advanced HNSCC consists of multimodality treatment comprising a combination of surgery, chemotherapy, and external beam radiation.[3–5] The disease prognosis significantly depends on the stage of the disease and site of the primary tumor, however, the survival rate of patients who have these solid aggressive tumors remains poor.[6] Moreover, the development of distant metastases, and therapy-resistant local and regional recurrences in these disease triggers high mortality rate. Despite better understanding of HNSCC tumor biology and targeted therapies, the efficacy of chemotherapy in HNSCC remains low and disease resistance is a major concern.[6, 7] To understand the tumor metabolism in head and neck cancer, most of the studies have been carried out on *in-vitro* culture of HNSCC cancer cells[1, 8, 9] and also on HNSCC tumor tissues *in-vivo*.[10, 11] In contrast, global analysis of human HNSCC tissues using a metabolomics approach provides a plethora of information which is highly useful in understanding the altered metabolism and in parallel, the altered metabolic biomarkers may potentially be useful for the early detection of HNSCC.

Nuclear magnetic resonance (NMR) spectroscopy and mass spectrometry (MS) are the two main analytical techniques highly suitable for metabolomics applications which exhibit different analytical strengths and weaknesses, and give complementary information.[12] With well-defined NMR protocols[13], it is possible to explore the metabolic profiling of biological fluids, tissue and cell extracts. NMR of tissue extracts has been employed to study the metabolic information of several types of cancer including breast[14, 15], prostate[16], brain[17, 18], lung[19] and colon cancer[20]. On the other hand, high-resolution magic-angle spinning (HR-MAS) NMR spectroscopy can be used for simultaneous detection of lipids as well as aqueous metabolites of intact tissues (without destruction) or cells[21] with a spectral resolution comparable to that of solution NMR spectroscopy; at the same time, MAS NMR technique maintain tissue integrity which can be further used for histopathological studies. Owing to its closer and realistic insights, the application of the HR-MAS technique has been increasing over the years for the analysis of intact tissues, predominantly in cancer research.[21] Most of the MAS NMR research studies focused on the discovery of potential metabolic biomarkers for different cancers representing brain[22, 23], prostate[24, 25], breast[26, 27], lung[28, 29], cervical[30, 31], colorectal[32], hepatic[33], renal[34, 35] and gastric cancer.[36] Multivariate statistical analyses on NMR spectral data of biological samples have been widely used to map the variations in global metabolic profiles and also to generate statistical models for improving adjunct diagnosis and/or prognosis. Due to technical ease of HR-MAS and vast diagnostic capabilities, recently, MAS NMR has been proposed for real-time diagnostics to monitor surgical patients.[37]

With reference to metabolic biomarker of HNSCC, the studies reported to date are based on ^{1}H NMR of serum[38], MAS NMR of tissues[39], and MS of urine[40] and saliva.[41] These metabolomics studies are useful; however they focused only on oral squamous cell

carcinoma, which is only one component of HNSCC. In this respect, the present study focused on the HR-MAS NMR metabolomic analysis of matched normal adjacent tissues (NAT) and tumor tissues representing classes of HNSCC which involved oral cavity, tongue, lip and larynx. In addition, HNSCC related lymph-node metastatic (LN-Met) tissues are also investigated in this study. We believe that this thorough HR-MAS NMR metabolic profiling study in combination with multivariate statistical analysis provides metabolic differentiation, which renders a more complete understanding of the biochemical insights of HNSCC. Further, this study provides metabolic information which may have significant importance in defining metabolic biomarkers of malignancy as a potential diagnostic/ prognostic value.

EXPERIMENTAL SECTION

Tissue sample collection and histopathological evaluation

Frozen HNSCC tissue specimens were obtained from ProteoGenex (ProteoGenex Inc., Culver City, CA, USA). A total of twenty-two HNSCC patients (16 males and 6 females with an age range of 39 – 88 years and mean age of 62.5 ± 11.6 years) were included in the present study. The patients' information, clinical diagnosis, TNM [extent of the tumor (T), the extent of spread to the lymph nodes (N), and the presence of distant metastasis (M)] staging system of world health organization and tumor grade established by histopathological evaluation are included in Table 1.

All tissues were snap-frozen in liquid nitrogen immediately after surgery and preserved at −80°C. In total, forty-three tissues (18 NAT, 18 tumor and 7 LN-Met) originated from tongue, oral cavity, lip, larynx and lymph-node of twenty-two HNSCC patients (Table 1) were investigated in the present study. Among these tissues, matched NAT and tumor tissues were obtained from 15 patients (No. 1–15); matched NAT, tumor and LN-Met tissues were taken from 3 patients (No. 16–18) and only LN-Met tissues were obtained from 4 patients (No.19–22).

High-Resolution MAS ^{1}H NMR

Each tissue sample (15–25 mg wet weight) was partially dissected from each specimen, rinsed with deuterium oxide (D_2O) (Sigma Aldrich) and inserted into a 4 mm zirconia MAS rotor (40 μL capacity) followed by the addition of ~10 μL D_2O, with excess fluid removed when assembling the Kel-F plastic cap. The total sample preparation time for each sample was < 5 min. All the NMR experiments on tissue samples were carried out on a Varian Inova 600 MHz NMR spectrometer equipped with gHX nano-probehead (Varian Inc.). All the ^{1}H HR-MAS spectra were acquired at 298 K. The spinning rate of the rotor was regulated by MAS controller (Varian Inc.) and also verified by measuring frequency separation between spinning side bands from ^{1}H spectra with an accuracy of ±1.0 Hz. Two sets of ^{1}H NMR spectra were acquired with a spinning rate of 2.6 kHz using a standard one-dimensional (1D) spectrum and a 1D Carr-Purcell-Meiboom-Gill (CPMG) spin-echo pulse sequence: $\pi/2\text{-}(\tau\text{-}\pi\text{-}\tau)_n$-acquisition-recycle delay. In both experiments, a spectral width of 8.5 KHz was used and water signal was pre-saturated using a weak continuous radio-frequency[2] irradiation on water resonance during the recycle delay. The free induction decay (FID) of CPMG spin-echo spectra were acquired into 32K data points during 1.98 s acquisition time with a 3 s recycle delay; 256 transients were coadded. T_2 filtering was obtained with an echo time of 100 μs (τ) repeated 320 times, resulting in an effective echo time of 64 ms ($2n\tau$). The total acquisition time for each sample was <30 min. The acquired data were processed using TOPSPIN 2.1 software (Bruker BioSpin, Karlsruhe, Germany). The FIDs were multiplied by an exponential window function with a line broadening factor of 0.3 Hz prior to Fourier transformation and the frequency domain spectra were manually phase and

baseline corrected. The proton chemical shifts were referenced to CH_3 signal of lactate at 1.33 ppm.

For chemical shift assignment of tissue metabolites, a two-dimensional (2D) ^{1}H-^{1}H total correlation spectroscopy (TOCSY) was performed on one of the tumor tissue samples. TOCSY spectra were acquired in the phase-sensitive mode using time proportional phase incrementation (TPPI) with MLEV17 spin-lock corresponding to mixing time of 80 ms. 2D TOCSY spectra were the resultant of 256 t_1 increments, co-addition of 16 scans each containing 2048 data points within 8.5 KHz spectral width, and a recycle delay of 1.5 s. The resulting data were zero filled to a 2048 × 1024 matrix and Fourier transformed along both dimensions after multiplying the data by a squared sine-bell window function shifted by $\pi/2$.

Multivariate Statistical Analysis

Before subjecting CPMG NMR spectra into multivariate statistical analysis, the chemical shift region of 0.7 – 8.5 ppm was converted to ASCII-files and the spectral regions of residual water 4.4–5.0 ppm and regions where spinning side bands appear (5.5 – 6.7 ppm) were excluded from the analysis. Spectral regions were normalized by the sum of all intensities over the entire sub-spectrum, and principal component analysis (PCA) and partial least square discriminant analysis (PLS-DA) were performed with mean-centered scaling (The Unscrambler V10.1, CAMO, Oslo, Norway). In the case of PLS-DA analysis, LN-Met tissues were included among the tumor group and analysis was carried out between NAT and tumor groups. The results were depicted by means of principal component scores plots (each point represents an individual sample), and loading plots in which metabolite peaks were shown as positive and negative signals to indicate differential changes of metabolites. The quality of the model was described by the cross-validation parameter R^2 and Q^2, representing the explained variance and the predictive capability of the model, respectively.

Relative Quantification and Statistical Analysis

Relative intensities of peaks from lipids and all the detected metabolites were determined using a selective non-overlapping signal of each metabolite from normalized spectra and results were represented as mean ± standard error of mean (mean ± SEM). Univariate statistical analysis was performed using the statistical software SPSS 11.5 (Statistical Package for Social Science, SPSS Inc.). Statistical significance of the metabolites between NAT, tumor and LN-Met tissues were analyzed by Mann-Whitney U-test and *P* values ≤0.05 were considered statistically significant.

Histopathological evaluation of HR-MAS NMR analyzed tissues

Following HR-MAS NMR analysis, tissue samples were immediately transferred from the MAS rotor to a fresh vial containing 10% formalin for histopathological processing. 5 μm section was cut from paraffin-embedded tissues and placed on histology slide, and stained with hematoxylin and eosin (H&E) using a standard protocol and evaluated by a pathologist.

RESULTS

HR-MAS ^{1}H NMR Spectroscopy

^{1}H MAS NMR analysis was performed on HNSCC derived tissues (N=43) consisting of 18 NAT, 18 tumor and 7 LN-Met tissues. In these samples, three patients (Table 1, patient numbers: 16, 17 and 18) contain matched NAT, tumor and LN-Met tissues. Among 43 tissue specimens, 3 tissues were not considered for further analysis for which histopathological diagnosis couldn't be evaluated due to the unavailability of epithelial tissue. To assess the metabolic stability of the tissues during an NMR experiment, two sequential ^{1}H CPMG NMR spectra were acquired from two samples at 298 K with a time gap of 30 min between

the data collection. No significant difference was detected in the metabolic pattern within 1 hr duration of NMR measurement, which is in agreement with previous observations for oral cancer[32] and other types of tissues.[29, 42, 43] Therefore, these results suggest that the tissues used in the present study were metabolically stable during NMR measurements at 298 K.

Representative ^{1}H CPMG NMR spectra of matched NAT and tumor tissues of oral cavity, tongue, lip and larynx are shown in Figure 1 and H&E photomicrograph of the corresponding post-NMR tissue is also shown alongside of each NMR spectrum. ^{1}H CPMG NMR spectra of matched NAT, tumor and LN-Met tissues from the same patient (No 18, Table 1) are shown in Figure 2 along with its H&E photomicrograph. NMR spectra of all the tissues showed intense signals of triglycerides (TG) which were not completely suppressed by the CPMG pulse sequence even at an effective echo time of 64 ms. In addition to signals from TG, some aqueous metabolites were also detected in all the NMR spectra except in one of the NAT sample (No 18), in which only TG signals (Figure 2a) were detected. The ^{1}H chemical shift of metabolites (Table S1, Supporting Information) were assigned based on the combination of previously published data of metabolites[44], comparing with ^{1}H spectra of authentic standards (Figure S1 and S2, Supporting Information) and 2D ^{1}H-^{1}H TOCSY spectrum. The metabolites detected were branched chain amino acids (BCAA) such as leucine (Leu), isoleucine (Ile) and valine (Val), alanine (Ala), lysine (Lys), glutamate (Glu), glutamine (Gln), aspartate (Asp), glycine (Gly), phenylalanine (Phe), tyrosine (Tyr), histidine (His), glutathione (GSH), choline-containing compounds (ChoCC) (choline, phosphocholine and glycerophosphocholine), lactate (Lac), acetate (Ac), creatine (Cre) and taurine (Tau).

Visual comparison of NMR spectra showed variable degrees of TG and aqueous metabolites; in general, most of the NAT samples showed higher levels of TG compared to tumor and LN-Met tissues (Figs.1 and 2). Though the NAT tissues investigated in this study were derived from different regions of head and neck, their ^{1}H NMR spectra are found to be identical (Figs.1 and 2). Similarly, ^{1}H NMR spectra of tumor tissues are also found to be identical, but were different from that of NAT samples (Figs.1 and 2). The average NMR spectrum (obtained from all normalized spectra) of all NAT, tumor and LN-Met tissues are shown in Figure S3 (in the Supporting Information).

Multivariate Statistical Analysis

To better understand the relationship of NMR metabolic pattern between NAT, tumor and LN-Met tissues, multivariate statistical analysis (PCA and PLS-DA) were performed. Figure 3 shows three-dimensional (3D) PCA score and PC1 loading plots of HR-MAS ^{1}H CPMG spectra of 40 tissues. In PCA score plot shown in Fig. 3A, the principal components PC1, PC2 and PC3 explained 86%, 6% and 2% variations in the spectra, respectively. A clear separation between NAT and tumor tissues was observed along PC1 and moreover LN-Met tissues were grouped among tumor tissues. Two samples each from tumor (indicated by red color arrows in Fig. 3A) and LN-Met (indicated by blue color arrows in Fig. 3A) tissues are grouped among NAT samples in Fig. 3A as they were diagnosed as poorly differentiated squamous cell carcinoma. Tissue samples from different tissue origins, namely head and neck, within NAT and tumor were indistinguishable, also separation due to tumor stage was not observed. PC1 loadings (Fig.3B) revealed lower levels of TG (positive values) and higher levels of amino acids, ChoCC, Lac, Ac, Cre and Tau in tumor and LN-Met tissues as compared to NAT.

3D PLS-DA score and loading plots of HR-MAS ^{1}H CPMG spectra of 40 tissues are included in Figure 3. PLS-DA score plot was characterized by $R^2 = 0.91$ and $Q^2 = 0.82$. This higher Q^2 value indicated good predictive capabilities of the model. The PLS-DA loading plots indicated all the detected metabolites contributing to the separation between the

groups. Receiver operator characteristic curve generated from predicted Y-values (Figure 4) showed an area under the curve of 0.867.

Relative Quantification of Metabolites and Statistical Analysis

Relative intensities of metabolites were calculated separately for NAT, tumor and LN-Met tissues using total area normalized spectra and presented as mean ± SEM. A selective non-overlapping resonance from each metabolite was used to calculate relative intensities: BCAA (0.93 – 1.07 ppm), Ala (1.45 – 1.51 ppm), Ac (1.91 – 1.93 ppm), Glu (2.31 – 2.40 ppm), Gln (2.42 – 2.49 ppm), GSH (2.51 – 2.61 ppm), Asp (2.62 – 2.72 ppm), Cre (3.02 – 3.07 ppm), Tau (3.39 – 3.47 ppm), Gly (3.55 – 3.57 ppm), Phe (7.30 – 7.46 ppm), and Tyr (6.85 – 6.92 ppm) were used. Since the triplet CH_2 signal of Tau (at 3.26 ppm) is overlapping with that of ChoCC, it is not possible to directly measure the intensity of peaks originating from ChoCC (Fig. 1). Therefore, to obtain the intensity of peaks from ChoCC, the intensity of another CH_2 triplet signal of Tau (3.39 – 3.47 ppm) was subtracted from the total intensity of all peaks in the chemical shift region of 3.16 – 3.31 ppm. Similarly, the CH_2 (4.12 ppm) signal of Lac was also overlapping with CH_2 (4.08 ppm) of TG; therefore Lac concentration was measured by subtracting the spectral region (4.04 – 4.15 ppm) with CH_2 (4.23 – 4.37 ppm) of TG. To calculate the total concentration of lipids –CO-CH_2 signal (2.20 – 2.29 ppm) was used.

Figure 5 shows bar plots of mean ± SEM and statistical significance (Mann-Whitney) of each metabolite from NAT, tumor and LN-Met tissues. It was observed that the TG levels were significantly decreased ($P < 0.001$) in both tumor and LN-Met as compared to NAT whereas all other detected metabolites were significantly increased ($P < 0.001$ for all) in tumor compared to NAT. In case of LN-Met tissues, metabolites such as Tau, ChoCC, BCAA, Ala, Glu, Asp, Cre, Gly were significantly increased ($P < 0.05$) as compared to NAT. A comparison of signal intensities measured from tumor and LN-Met samples (Fig. 5) suggests that there is no significant difference in metabolites identified from these two types of tissues.

Histopathological assessment of tissues after NMR experiments

After MAS NMR experiments, histopathological (H & E) assessments were performed for all the tissue samples. The standard TNM classification, grade and stage of tumor are presented in Table 1. Representative photomicrographs of matched NAT and the corresponding tumor tissues of oral cavity, tongue, lip and larynx are shown alongside of each NMR spectrum in Figure 1, and matched NAT, tumor and LN-Met tissue from a single patient (Table 1, No.18) are shown in Figure 2. All the NAT demonstrate parakeratinized stratified squamous epithelium and underlying fibrovascular connective tissue. Tumor and LN-Met tissues represent squamous cell carcinoma with neoplastic cells demonstrating varying degrees of epithelial differentiation invade the adjacent connective tissue predominantly as nests, sheets or single cells. Prominent keratin production in the form of keratin pearls was observed in case No.2 and 18, a lymphoid aggregate associated with tumor cells was observed in No. 16 (metastatic tissue) and prominent comedo necrosis was observed in case No.21.

DISCUSSION

The HR-MAS NMR has becoming an important tool for investigating the metabolism involved in the malignant transformation. Particularly, the ability of MAS NMR in differentiating metabolic phenotypes of normal and tumor tissues within a few minutes of experimental duration make the technique amenable for clinical diagnostics/prognostics of cancer. Over the years, the technical capabilities of MAS NMR have been explored in

understanding biochemical insights and differentiating many cancer types. More recently, Kinross et al[37] proposed MAS NMR for real-time diagnostics to monitor surgical patients. In the present study, HR-NMR based metabolic profiling was undertaken to understand the biochemical insights of tumor biology and also to delineate the candidate biomarkers of HNSCC. To the best of our knowledge this is the first comprehensive MAS NMR study of HNSCC involving tissues from oral cavity, lip, tongue and larynx. We believe that the dysregulation of metabolites investigated using ^{1}H MAS NMR combined with multivariate statistical analysis could serve as an adjunct tool for clinical differentiation of HNSCC tissues and further understanding of HNSCC metabolism.

The present study clearly showed alterations in TG levels and several other aqueous metabolites in tumor as compared to NAT, also LN-Met tissues showed similar changes as observed in tumor. In addition, HR-MAS spectra of tissues from various sites of head and neck cancer (oral cavity, lip, tongue and larynx) were indistinguishable within their NAT and tumor tissues. This result demonstrates that this group of tissues adopt identical metabolism during their malignant transformation. Our results also suggest that HR-MAS experiments can differentiate the metabotypes of NAT, tumor and LN-Met tissues with a high AUC value (0.867). In this respect, HR-MAS NMR can be used as an adjunct tool for differentiation of HNSCC from normal tissues along with gold standard histopathological analysis; nevertheless MAS NMR is still finding its day to stand as a full-fledged tool in clinical diagnosis. Further, the observed perturbations in TG and metabolites and the related metabolism provide further understanding of HNSCC tumor biology.

Highly Active Glycolysis

Our HR-MAS results show increased levels of lactate, alanine and glycine in tumor and LN-Met as compared to NAT. Lactate is an end product of glycolysis which shows elevation during tissue hypoxia and ischemia.[45] Elevated lactate levels have been observed in wide variety of tumors and therefore lactate has been considered as a universal biomarker of malignancy. Most tumors have the ability to break down glucose by glycolysis at a vastly higher rate than in normal tissues, even in the presence of high oxygen, the phenomenon known as Warburg effect.[46] Interestingly, in the present study, glucose, the precursor in glycolysis is not detected in any of the head and neck and lymph node metastatic tissues. However, it has been shown in HNSCC that glucose entry into the cell is facilitated by GLUT1- and GLUT3-mediated glucose transporters and is involved in the increased glucose metabolism.[47] On the other hand, elevated glycine could be attributed to increased activity of 3-phosphoglycerate dehydrogenase, which catalyzes the formation of the glycine for *de novo* purine and pyrimidine biosynthesis. Also, glycine is a precursor of sarcosine (N-methyl glycine), which was shown to be a potential metabolic biomarker for aggressive prostate cancer.[48] Elevated glycine has also been reported in a MAS NMR study of human colorectal cancer[32], which is consistent with the increased activity of 3-phosphoglycerate dehydrogenase observed in human colon carcinoma and rat sarcoma.[49] Elevated level of alanine, which is also another important end product of glycolysis/glutaminolysis, was found in HNSCC and metastatic tissues and it has been found to be a major source of energy in tumor proliferation and growth. Recent studies reported that the change in lactate and alanine can act as an important parameter for monitoring tumor aggressiveness in prostate cancer[50] and prognosis for lung cancer.[51] We believe that monitoring the changes of these two metabolites could also be used as *in-vivo* diagnostic/prognostic marker in HNSCC. Taken together, the observed increase in the levels of lactate, alanine and glycine suggests that glycolytic pathway is highly active in HNSCC similar to other tumor types. Furthermore, the creatine level in tumor and LN-Met tissues was elevated which can be attributed to the alteration in energy metabolism. A significant down-regulation of creatine

kinase reported in oral squamous cell carcinoma[52] further supports our observation of elevated level of creatine.

Amino Acids Metabolism

Our HR-MAS results showed increased levels of glutamine, glutamate, aspartate and alanine in tumor and LN-Met tissues, which suggest that in addition to glucose, HNSCC cells could also depend on glutaminolysis for carbon and nitrogen source. Elevated levels of glutamine and glutamate were also reported by a MAS NMR study of hepatocellular carcinoma.[33] These observations indicate that glutaminolysis allows cancer cells to maintain a sufficient anaplerotic flux (entry of substrate other than acteylCoA into the tricarboxylic acid cycle) that produce glutamate and α-ketoglutarate molecules to use as a source of carbon for the tricarboxylic acid cycle. Also, it has been shown using NMR experiments that glutamine is a major anaplerotic precursor in proliferating glioma cells in both rats[53] and humans.[54] However, a recent report on *in-vitro* culture of HNSCC cell lines shows that only glucose (not glutamine) is the dominant energy source required for proliferation and growth[55], therefore the exact role of glutaminolysis is unclear in HNSCC.

Elevated BCAA, phenylalanine, tyrosine and taurine were observed both in tumor and LN-Met tissues, and also observed in other tumor types. The BCAA were involved in anaplerosis during tumor cell proliferation and growth. It has been demonstrated that tumor cells increase the oxidation of BCAA increases in the host,[56, 57] which may be a contributing factor of cancer cachexia. Similarly, phenylalaine and tyrosine could also be involved in anaplerosis, which enters the tricarboxylic acid cycle by converting into fumarate. By and large, it appears that the physiological state of HNSCC involves a large influx of amino acids into the tricarboxylic acid cycle. Taurine is an osmoprotectant and its increased level was observed in the present study and also reported from studies on other tumors.[30, 32] Taurine was suggested as a biomarker of apoptosis in glial tumors[58] and also for cancer therapy due to its antioxidant and antiangiogenic properties[59]. Owing to multitude functions of taurine, its exact role in HNSCC is not clear. Nevertheless, elevated taurine could be attributed to an endogenous defense mechanism against tumor proliferation.

Lipid metabolism

In the present study, MAS NMR results clearly showed decreased levels of TG in tumor and LN-Met tissues compared to NAT. The decreased TG levels were also reported in MAS NMR studies of colorectal[32] and oral cancer.[39] The correlation between TG metabolism and cancer is unclear; however, it could be hypothesized that the lipolysis of TG into fatty acids may occur in tumor cells, a factor which leads to cancer-associated cachexia.[60] Further, the fatty acids may undergo β-oxidation into acetyl-CoA. In addition to abnormally high rate of glycolysis (Warburg effect)[46], tumor cells also show increased fatty acid metabolism[61], in which oxidation of a fatty acid may exist to deliver bioenergy for rapid tumor cells proliferation and growth. Therefore, the lower lipid levels particularly triglycerides and fatty acids in HNSCC tissues could be associated with increased demand of lipids for membrane biosynthesis of tumor cells leading to a higher utilization rate of lipids. Taken together, HNSCC may be associated with the alteration of lipid metabolism facilitated by lipolysis of triglycerides and concomitant fatty acid oxidation.

Membrane Choline phospholipid metabolism

ChoCC were also found elevated in tumor and LN-Met tissues. These important molecules are precursors of cell membrane have been found elevated in most of the MAS NMR studies of various tumors types and the increase in these metabolites reflect the cell death (apoptosis and necrosis) and proliferation. The increase in ChoCC has been associated with progressive alteration of membrane choline phospholipid metabolism during malignant

transformation.[62] It has been reported that the activity of phosphatidylcholine-specific phospholipase C (PLC) and phospholipase D (PLD), the enzymes responsible for the degradation of phosphatidylcholine was higher in human mammary epithelial and epithelial ovarian carcinoma cell lines.[62, 63] These findings suggest that both biosynthetic and catabolic pathways of the phosphatidylcholine cycle contribute to the accumulation of ChoCC in tumor tissues. Due to a strong association of these phospholipases (choline kinase, PLC, PLD) in malignant transformation of most of the human cancers, these enzymes may provide molecular targets for anticancer chemotherapies.[64] The alteration in the levels of ChoCC compounds were detected *in-vivo* in breast cancer patients using quantitative MRS techniques and used for the diagnosis/prognosis of breast cancer.[65] We believe that measurement of ChoCC in HNSCC patients by quantitative MRS could act as important biomarkers for the diagnosis /prognosis of HNSCC.

Oxidative Stress

In the present study, HR-MAS measurements also showed elevated GSH levels in tumor and LN-Met tissues compared to NAT. The tripeptide, GSH is a ubiquitous intra- and extracellular protective antioxidant against oxidative/nitrosative stress, which plays a vital role against pro-inflammatory processes.[66] The antioxidant GSH has been shown to be critical in protecting airspace epithelium from oxidative/free radical mediated injury and inflammation[66], and also in cancer.[67] Several studies suggest that cancer cells undergo increased oxidative stress associated with malignant transformation, alterations in metabolic activity, and increased generation of reactive oxygen species.[68] The increased oxidative stress in cancer cells could likely to cause the elevated expression of antioxidant enzymes such as glutathione peroxidase, glutathione reductase and glutathione-S-transferase. The elevated expression of GSH, glutathione peroxidase and glutatione reductase were reported in the tissues of oral squamous cell carcinoma[69, 70] and other various human cancer such as colorectal, breast, ovarian and brain tumor.[68] In contrast, the decreased levels of GSH and these antioxidant enzymes were observed in plasma[70–72] of oral cancer patients. Therefore, the elevated GSH levels could be attributed enhanced antioxidant mechanism in HNSCC tissues. Furthermore, the enhanced antioxidant events in tumor tissues make them less susceptible to oxidative stress, which may be an added advantage to tumor cells for a selective growth. Taken together, the observed higher GSH levels in the present study could be helpful in further understanding of oxidative stress mechanism in HNSCC biology.

CONCLUSION

The present HR-MAS NMR study clearly differentiated metabolic phenotypes of HNSCC and NAT, and LN-Met tissues showed metabolic pattern similar to that of HNSCC tissues. Both HNSCC and LN-Met tissues are highlighted by the increased levels of branched chain amino acids, lactate, alanine, glutamine, glutamate, glutathione, aspartate, creatine, choline containing compounds, taurine, phenylalanine and tyrosine, and decreased levels of triglycerides. Tumor tissues from various anatomical sites (tongue, lip, oral cavity and larynx) of head and neck displayed a similar metabolic state which suggests that these groups of HNSCC tissues follow similar metabolism during malignant transformation and growth. The results revealed multiple metabolic alterations in tumor tissues which include highly active glycolysis, increased influx of amino acids (anaplerosis) into the tricarboxylic acid cycle, membrane choline phospholipid metabolism, oxidative and osmotic stress mechanisms. Moreover, decreased levels of TG may indicate lipolysis of TG and concomitant β-oxidation of fatty acids which may exist to deliver bioenergy for rapid tumor cells proliferation and growth. The present metabolomics study also demonstrated that HR-MAS NMR based metabolic profiling coupled with multivariate statistical analysis can be used as a diagnostic tool (in conjunction with histopathology) for differentiating HNSCC

from NAT. We believe that monitoring the significant metabolites noted in the present study could potentially be used as a non-invasive diagnostic/prognostic marker in HNSCC using *in-vivo* MRS studies.

Supplementary Material

Refer to Web version on PubMed Central for supplementary material.

Acknowledgments

This research was supported by funds from NIH (RR023587 to A. R and R01DE014429 and R56DE014429 to Y.L.K)

REFERENCES

1. Schmitz S, Machiels JP. Molecular biology of squamous cell carcinoma of the head and neck: relevance and therapeutic implications. Expert Rev Anticancer Ther. 2010; 10(9):1471–1484. [PubMed: 20836682]
2. http://www.cancer.org/Research/CancerFactsFigures/CancerFactsFigures/cancer-facts-figures-2011, In.
3. Forastiere A, Weber R, Ang K. Treatment of head and neck cancer. N Engl J Med. 2008; 358(10): 1076. author reply 1077-8. [PubMed: 18322293]
4. Forastiere AA. Chemotherapy in the treatment of locally advanced head and neck cancer. J Surg Oncol. 2008; 97(8):701–707. [PubMed: 18493921]
5. Forastiere AA, Trotti A, Pfister DG, Grandis JR. Head and neck cancer: recent advances and new standards of care. J Clin Oncol. 2006; 24(17):2603–2605. [PubMed: 16763271]
6. Pignon JP, le Maitre A, Maillard E, Bourhis J. Meta-analysis of chemotherapy in head and neck cancer (MACH-NC): an update on 93 randomised trials and 17,346 patients. Radiother Oncol. 2009; 92(1):4–14. [PubMed: 19446902]
7. Bernier J, Bentzen SM, Vermorken JB. Molecular therapy in head and neck oncology. Nat Rev Clin Oncol. 2009; 6(5):266–277. [PubMed: 19390553]
8. Sandulache VC, Ow TJ, Pickering CR, Frederick MJ, Zhou G, Fokt I, Davis-Malesevich M, Priebe W, Myers JN. Glucose, not glutamine, is the dominant energy source required for proliferation and survival of head and neck squamous carcinoma cells. Cancer. 2011; 117(13):2926–2938. [PubMed: 21692052]
9. Jiffar T, Yilmaz T, Lee J, Hanna E, El-Naggar A, Yu D, Myers JN, Kupferman ME. KiSS1 mediates platinum sensitivity and metastasis suppression in head and neck squamous cell carcinoma. Oncogene. 2011
10. Karahatay S, Thomas K, Koybasi S, Senkal CE, Elojeimy S, Liu X, Bielawski J, Day TA, Gillespie MB, Sinha D, Norris JS, Hannun YA, Ogretmen B. Clinical relevance of ceramide metabolism in the pathogenesis of human head and neck squamous cell carcinoma (HNSCC): attenuation of C(18)-ceramide in HNSCC tumors correlates with lymphovascular invasion and nodal metastasis. Cancer Lett. 2007; 256(1):101–111. [PubMed: 17619081]
11. Ziebart T, Walenta S, Kunkel M, Reichert TE, Wagner W, Mueller-Klieser W. Metabolic and proteomic differentials in head and neck squamous cell carcinomas and normal gingival tissue. J Cancer Res Clin Oncol. 2011; 137(2):193–199. [PubMed: 20383719]
12. Lindon JC, Nicholson JK. Spectroscopic and statistical techniques for information recovery in metabonomics and metabolomics. Annu Rev Anal Chem (Palo Alto Calif). 2008; 1:45–69. [PubMed: 20636074]
13. Beckonert O, Keun HC, Ebbels TM, Bundy J, Holmes E, Lindon JC, Nicholson JK. Metabolic profiling, metabolomic and metabonomic procedures for NMR spectroscopy of urine, plasma, serum and tissue extracts. Nat Protoc. 2007; 2(11):2692–2703. [PubMed: 18007604]

14. Gribbestad IS, Petersen SB, Fjosne HE, Kvinnsland S, Krane J. 1H NMR spectroscopic characterization of perchloric acid extracts from breast carcinomas and non-involved breast tissue. NMR Biomed. 1994; 7(4):181–194. [PubMed: 7946996]
15. Beckonert O, Monnerjahn J, Bonk U, Leibfritz D. Visualizing metabolic changes in breast-cancer tissue using 1H-NMR spectroscopy and self-organizing maps. NMR Biomed. 2003; 16(1):1–11. [PubMed: 12577292]
16. Fowler AH, Pappas AA, Holder JC, Finkbeiner AE, Dalrymple GV, Mullins MS, Sprigg JR, Komoroski RA. Differentiation of human prostate cancer from benign hypertrophy by in vitro 1H NMR. Magn Reson Med. 1992; 25(1):140–147. [PubMed: 1375702]
17. Maxwell RJ, Martinez-Perez I, Cerdan S, Cabanas ME, Arus C, Moreno A, Capdevila A, Ferrer E, Bartomeus F, Aparicio A, Conesa G, Roda JM, Carceller F, Pascual JM, Howells SL, Mazucco R, Griffiths JR. Pattern recognition analysis of 1H NMR spectra from perchloric acid extracts of human brain tumor biopsies. Magn Reson Med. 1998; 39(6):869–877. [PubMed: 9621910]
18. Lehnhardt FG, Rohn G, Ernestus RI, Grune M, Hoehn M. 1H- and (31)P-MR spectroscopy of primary and recurrent human brain tumors in vitro: malignancy-characteristic profiles of water soluble and lipophilic spectral components. NMR Biomed. 2001; 14(5):307–317. [PubMed: 11477651]
19. Hanaoka H, Yoshioka Y, Ito I, Niitu K, Yasuda N. In vitro characterization of lung cancers by the use of 1H nuclear magnetic resonance spectroscopy of tissue extracts and discriminant factor analysis. Magn Reson Med. 1993; 29(4):436–440. [PubMed: 8385259]
20. Moreno A, Arus C. Quantitative and qualitative characterization of 1H NMR spectra of colon tumors, normal mucosa and their perchloric acid extracts: decreased levels of myo-inositol in tumours can be detected in intact biopsies. NMR Biomed. 1996; 9(1):33–45. [PubMed: 8842031]
21. Beckonert O, Coen M, Keun HC, Wang Y, Ebbels TM, Holmes E, Lindon JC, Nicholson JK. High-resolution magic-angle-spinning NMR spectroscopy for metabolic profiling of intact tissues. Nat Protoc. 2010; 5(6):1019–1032. [PubMed: 20539278]
22. Monleon D, Morales JM, Gonzalez-Darder J, Talamantes F, Cortes O, Gil-Benso R, Lopez-Gines C, Cerda-Nicolas M, Celda B. Benign and atypical meningioma metabolic signatures by high-resolution magic-angle spinning molecular profiling. J Proteome Res. 2008; 7(7):2882–2888. [PubMed: 18507434]
23. Erb G, Elbayed K, Piotto M, Raya J, Neuville A, Mohr M, Maitrot D, Kehrli P, Namer IJ. Toward improved grading of malignancy in oligodendrogliomas using metabolomics. Magn Reson Med. 2008; 59(5):959–965. [PubMed: 18429037]
24. Tessem MB, Swanson MG, Keshari KR, Albers MJ, Joun D, Tabatabai ZL, Simko JP, Shinohara K, Nelson SJ, Vigneron DB, Gribbestad IS, Kurhanewicz J. Evaluation of lactate and alanine as metabolic biomarkers of prostate cancer using 1H HR-MAS spectroscopy of biopsy tissues. Magn Reson Med. 2008; 60(3):510–516. [PubMed: 18727052]
25. Cheng LL, Burns MA, Taylor JL, He W, Halpern EF, McDougal WS, Wu CL. Metabolic characterization of human prostate cancer with tissue magnetic resonance spectroscopy. Cancer Res. 2005; 65(8):3030–3034. [PubMed: 15833828]
26. Sitter B, Lundgren S, Bathen TF, Halgunset J, Fjosne HE, Gribbestad IS. Comparison of HR MAS MR spectroscopic profiles of breast cancer tissue with clinical parameters. NMR Biomed. 2006; 19(1):30–40. [PubMed: 16229059]
27. Bathen TF, Jensen LR, Sitter B, Fjosne HE, Halgunset J, Axelson DE, Gribbestad IS, Lundgren S. MR-determined metabolic phenotype of breast cancer in prediction of lymphatic spread, grade, and hormone status. Breast Cancer Res Treat. 2007; 104(2):181–189. [PubMed: 17061040]
28. Chen W, Zu Y, Huang Q, Chen F, Wang G, Lan W, Bai C, Lu S, Yue Y, Deng F. Study on metabonomic characteristics of human lung cancer using high resolution magic-angle spinning (1) H NMR spectroscopy and multivariate data analysis. Magn Reson Med. 2011
29. Rocha CM, Barros AS, Gil AM, Goodfellow BJ, Humpfer E, Spraul M, Carreira IM, Melo JB, Bernardo J, Gomes A, Sousa V, Carvalho L, Duarte IF. Metabolic profiling of human lung cancer tissue by 1H high resolution magic angle spinning (HRMAS) NMR spectroscopy. J Proteome Res. 2010; 9(1):319–332. [PubMed: 19908917]

30. Sitter B, Bathen T, Hagen B, Arentz C, Skjeldestad FE, Gribbestad IS. Cervical cancer tissue characterized by high-resolution magic angle spinning MR spectroscopy. Magma. 2004; 16(4): 174–181. [PubMed: 14999565]

31. De Silva SS, Payne GS, Thomas V, Carter PG, Ind TE, deSouza NM. Investigation of metabolite changes in the transition from pre-invasive to invasive cervical cancer measured using (1)H and (31)P magic angle spinning MRS of intact tissue. NMR Biomed. 2009; 22(2):191–198. [PubMed: 18833545]

32. Chan EC, Koh PK, Mal M, Cheah PY, Eu KW, Backshall A, Cavill R, Nicholson JK, Keun HC. Metabolic profiling of human colorectal cancer using high-resolution magic angle spinning nuclear magnetic resonance (HR-MAS NMR) spectroscopy and gas chromatography mass spectrometry (GC/MS). J Proteome Res. 2009; 8(1):352–361. [PubMed: 19063642]

33. Yang Y, Li C, Nie X, Feng X, Chen W, Yue Y, Tang H, Deng F. Metabonomic studies of human hepatocellular carcinoma using high-resolution magic-angle spinning 1H NMR spectroscopy in conjunction with multivariate data analysis. J Proteome Res. 2007; 6(7):2605–2614. [PubMed: 17564425]

34. Tate AR, Foxall PJ, Holmes E, Moka D, Spraul M, Nicholson JK, Lindon JC. Distinction between normal and renal cell carcinoma kidney cortical biopsy samples using pattern recognition of (1)H magic angle spinning (MAS) NMR spectra. NMR Biomed. 2000; 13(2):64–71. [PubMed: 10797634]

35. Righi V, Mucci A, Schenetti L, Tosi MR, Grigioni WF, Corti B, Bertaccini A, Franceschelli A, Sanguedolce F, Schiavina R, Martorana G, Tugnoli V. Ex vivo HR-MAS magnetic resonance spectroscopy of normal and malignant human renal tissues. Anticancer Res. 2007; 27(5A):3195–3204. [PubMed: 17970061]

36. Tugnoli V, Mucci A, Schenetti L, Righi V, Calabrese C, Fabbri A, Di Febo G, Tosi MR. Ex vivo HR-MAS Magnetic Resonance Spectroscopy of human gastric adenocarcinomas: a comparison with healthy gastric mucosa. Oncol Rep. 2006; 16(3):543–553. [PubMed: 16865254]

37. Kinross JM, Holmes E, Darzi AW, Nicholson JK. Metabolic phenotyping for monitoring surgical patients. Lancet. 2011; 377(9780):1817–1819. [PubMed: 21596428]

38. Tiziani S, Lopes V, Gunther UL. Early stage diagnosis of oral cancer using 1H NMR-based metabolomics. Neoplasia. 2009; 11(3):269–276. 4p following 269. [PubMed: 19242608]

39. Srivastava S, Roy R, Gupta V, Tiwari A, Srivastava AN, Sonkar A. Proton HR-MAS MR spectroscopy of oral squamous cell carcinoma tissues: an ex vivo study to identify malignancy induced metabolic fingerprints. Metabolomics. 2011; 7(2):278–288.

40. Xie GX, Chen TL, Qiu YP, Shi P, Zheng XJ, Su MM, Zhao AH, Zhou ZT, Jia W. Urine metabolite profiling offers potential early diagnosis of oral cancer. Metabolomics. 2011 Published Online: 23 April.

41. Sugimoto M, Wong DT, Hirayama A, Soga T, Tomita M. Capillary electrophoresis mass spectrometry-based saliva metabolomics identified oral, breast and pancreatic cancer-specific profiles. Metabolomics. 2010; 6(1):78–95. [PubMed: 20300169]

42. Swanson MG, Zektzer AS, Tabatabai ZL, Simko J, Jarso S, Keshari KR, Schmitt L, Carroll PR, Shinohara K, Vigneron DB, Kurhanewicz J. Quantitative analysis of prostate metabolites using 1H HR-MAS spectroscopy. Magn Reson Med. 2006; 55(6):1257–1264. [PubMed: 16685733]

43. Opstad KS, Bell BA, Griffiths JR, Howe FA. An assessment of the effects of sample ischaemia and spinning time on the metabolic profile of brain tumour biopsy specimens as determined by high-resolution magic angle spinning (1)H NMR. NMR Biomed. 2008; 21(10):1138–1147. [PubMed: 18666093]

44. Tugnoli V, Schenetti L, Mucci A, Parenti F, Cagnoli R, Righi V, Trinchero A, Nocetti L, Toraci C, Mavilla L, Trentini G, Zunarelli E, Tosi MR. Ex vivo HR-MAS MRS of human meningiomas: a comparison with in vivo 1H MR spectra. Int J Mol Med. 2006; 18(5):859–869. [PubMed: 17016616]

45. De Backer D. Lactic acidosis. Intensive Care Med. 2003; 29(5):699–702. [PubMed: 12682722]

46. Warburg O, Posener K, Negelein E. On the metabolism of carcinoma cells. Biochem Z. 1924; 152:309–344.

47. Mellanen P, Minn H, Grenman R, Harkonen P. Expression of glucose transporters in head-and-neck tumors. International journal of cancer. Journal international du cancer. 1994; 56(5):622–629. [PubMed: 8314336]
48. Sreekumar A, Poisson LM, Rajendiran TM, Khan AP, Cao Q, Yu J, Laxman B, Mehra R, Lonigro RJ, Li Y, Nyati MK, Ahsan A, Kalyana-Sundaram S, Han B, Cao X, Byun J, Omenn GS, Ghosh D, Pennathur S, Alexander DC, Berger A, Shuster JR, Wei JT, Varambally S, Beecher C, Chinnaiyan AM. Metabolomic profiles delineate potential role for sarcosine in prostate cancer progression. Nature. 2009; 457(7231):910–914. [PubMed: 19212411]
49. Snell K, Natsumeda Y, Eble JN, Glover JL, Weber G. Enzymic imbalance in serine metabolism in human colon carcinoma and rat sarcoma. Brit J Cancer. 1988; 57(1):87–90. [PubMed: 3126791]
50. Yaligar J, Thakur SB, Bokacheva L, Carlin S, Thaler HT, Rizwan A, Lupu ME, Wang Y, Matei CC, Zakian KL, Koutcher JA. Lactate MRSI and DCE MRI as surrogate markers of prostate tumor aggressiveness. NMR Biomed. 2011
51. Yokota H, Guo J, Matoba M, Higashi K, Tonami H, Nagao Y. Lactate, choline, and creatine levels measured by vitro 1H-MRS as prognostic parameters in patients with non-small-cell lung cancer. J Magn Reson Imaging. 2007; 25(5):992–999. [PubMed: 17410583]
52. Onda T, Uzawa K, Endo Y, Bukawa H, Yokoe H, Shibahara T, Tanzawa H. Ubiquitous mitochondrial creatine kinase downregulated in oral squamous cell carcinoma. Brit J Cancer. 2006; 94(5):698–709. [PubMed: 16479256]
53. Portais JC, Voisin P, Merle M, Canioni P. Glucose and glutamine metabolism in C6 glioma cells studied by carbon 13 NMR. Biochimie. 1996; 78(3):155–164. [PubMed: 8831946]
54. DeBerardinis RJ, Mancuso A, Daikhin E, Nissim I, Yudkoff M, Wehrli S, Thompson CB. Beyond aerobic glycolysis: transformed cells can engage in glutamine metabolism that exceeds the requirement for protein and nucleotide synthesis. Proc Natl Acad Sci U S A. 2007; 104(49): 19345–19350. [PubMed: 18032601]
55. Sandulache VC, Ow TJ, Pickering CR, Frederick MJ, Zhou G, Fokt I, Davis-Malesevich M, Priebe W, Myers JN. Glucose, not glutamine, is the dominant energy source required for proliferation and survival of head and neck squamous carcinoma cells. Cancer. 2011
56. Lazo PA. Tumour induction of host leucine starvation. FEBS Lett. 1981; 135(2):229–231. [PubMed: 7319047]
57. Argiles JM, Lopez-Soriano FJ. The oxidation of leucine in tumour-bearing rats. Biochem J. 1990; 268(1):241–244. [PubMed: 2111700]
58. Opstad KS, Bell BA, Griffiths JR, Howe FA. Taurine: a potential marker of apoptosis in gliomas. Brit J Cancer. 2009; 100(5):789–794. [PubMed: 19223899]
59. El Agouza IM, Eissa SS, El Houseini MM, El-Nashar DE, Abd El Hameed OM. Taurine: a novel tumor marker for enhanced detection of breast cancer among female patients. Angiogenesis. 2011
60. Das SK, Eder S, Schauer S, Diwoky C, Temmel H, Guertl B, Gorkiewicz G, Tamilarasan KP, Kumari P, Trauner M, Zimmermann R, Vesely P, Haemmerle G, Zechner R, Hoefler G. Adipose triglyceride lipase contributes to cancer-associated cachexia. Science. 2011; 333(6039):233–238. [PubMed: 21680814]
61. Kuhajda FP. Fatty-acid synthase and human cancer: new perspectives on its role in tumor biology. Nutrition. 2000; 16(3):202–208. [PubMed: 10705076]
62. Aboagye EO, Bhujwalla ZM. Malignant transformation alters membrane choline phospholipid metabolism of human mammary epithelial cells. Cancer Res. 1999; 59(1):80–84. [PubMed: 9892190]
63. Iorio E, Mezzanzanica D, Alberti P, Spadaro F, Ramoni C, D'Ascenzo S, Millimaggi D, Pavan A, Dolo V, Canevari S, Podo F. Alterations of choline phospholipid metabolism in ovarian tumor progression. Cancer Res. 2005; 65(20):9369–9376. [PubMed: 16230400]
64. Glunde K, Serkova NJ. Therapeutic targets and biomarkers identified in cancer choline phospholipid metabolism. Pharmacogenomics. 2006; 7(7):1109–1123. [PubMed: 17054420]
65. Bolan PJ, Meisamy S, Baker EH, Lin J, Emory T, Nelson M, Everson LI, Yee D, Garwood M. In vivo quantification of choline compounds in the breast with 1H MR spectroscopy. Magn Reson Med. 2003; 50(6):1134–1143. [PubMed: 14648561]

66. Rahman I, MacNee W. Oxidative stress and regulation of glutathione in lung inflammation. Eur Respir J. 2000; 16(3):534–554. [PubMed: 11028671]

67. Valko M, Rhodes CJ, Moncol J, Izakovic M, Mazur M. Free radicals, metals and antioxidants in oxidative stress-induced cancer. Chem Biol Interact. 2006; 160(1):1–40. [PubMed: 16430879]

68. Pelicano H, Carney D, Huang P. ROS stress in cancer cells and therapeutic implications. Drug Resist Updat. 2004; 7(2):97–110. [PubMed: 15158766]

69. Wong DY, Hsiao YL, Poon CK, Kwan PC, Chao SY, Chou ST, Yang CS. Glutathione concentration in oral cancer tissues. Cancer Lett. 1994; 81(2):111–116. [PubMed: 8012928]

70. Fiaschi AI, Cozzolino A, Ruggiero G, Giorgi G. Glutathione, ascorbic acid and antioxidant enzymes in the tumor tissue and blood of patients with oral squamous cell carcinoma. Eur Rev Med Pharmacol Sci. 2005; 9(6):361–367. [PubMed: 16479741]

71. Manoharan S, Kolanjiappan K, Suresh K, Panjamurthy K. Lipid peroxidation & antioxidants status in patients with oral squamous cell carcinoma. Indian J Med Res. 2005; 122(6):529–534. [PubMed: 16518005]

72. Beevi SS, Rasheed AM, Geetha A. Evaluation of oxidative stress and nitric oxide levels in patients with oral cavity cancer. Jpn J Clin Oncol. 2004; 34(7):379–385. [PubMed: 15342664]

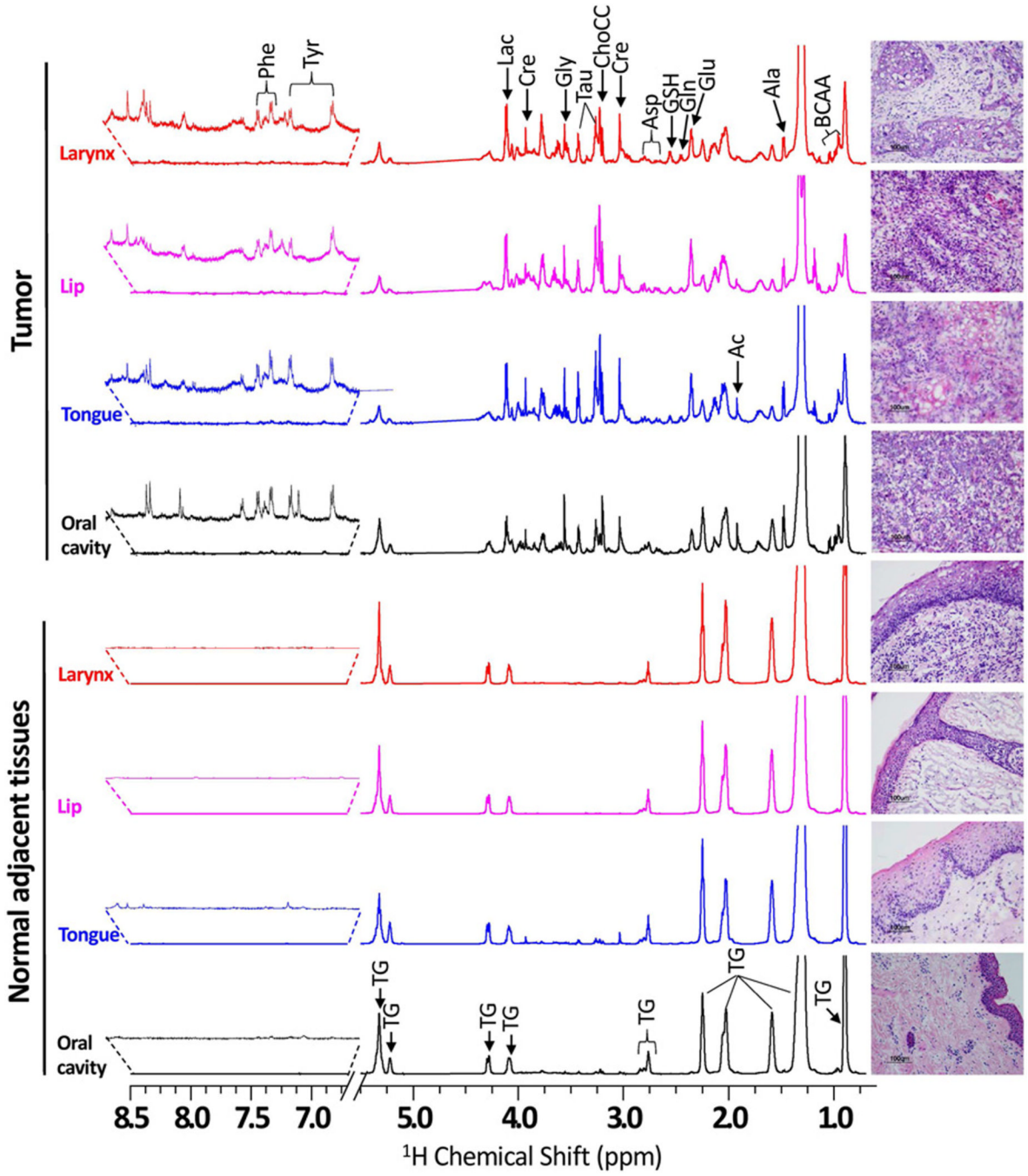

Figure 1.

Representative 600 MHz ^{1}H HR-MAS CPMG NMR spectra (area normalized) of matched NAT and HNSCC tissues from various anatomical sites of head and neck involving oral cavity, tongue, lip and larynx of four different patients. The vertical scales of all the spectra were kept the same and the chemical shift region from 5.2 – 6.5 ppm (spinning side bands) is not shown in all the spectra. The intensity of peak in the chemical shift region 6.7 – 8.5 ppm was increased equally in all spectra to show the low-abundant taurine and phenylalanine. The triglyceride signals were indicated as 'TG'. The corresponding H&E photomicrographs of post HR-MAS NMR tissues are shown alongside of each ^{1}H CPMG spectrum. All the NAT are composed of parakeratinized stratified squamous epithelium and

underlying fibrovascular connective tissue. However, tumor tissues were composed of squamous cell carcinomas with neoplastic cells demonstrating varying degrees of epithelial differentiation invade the adjacent connective tissue predominantly as nests, sheets or single cells.

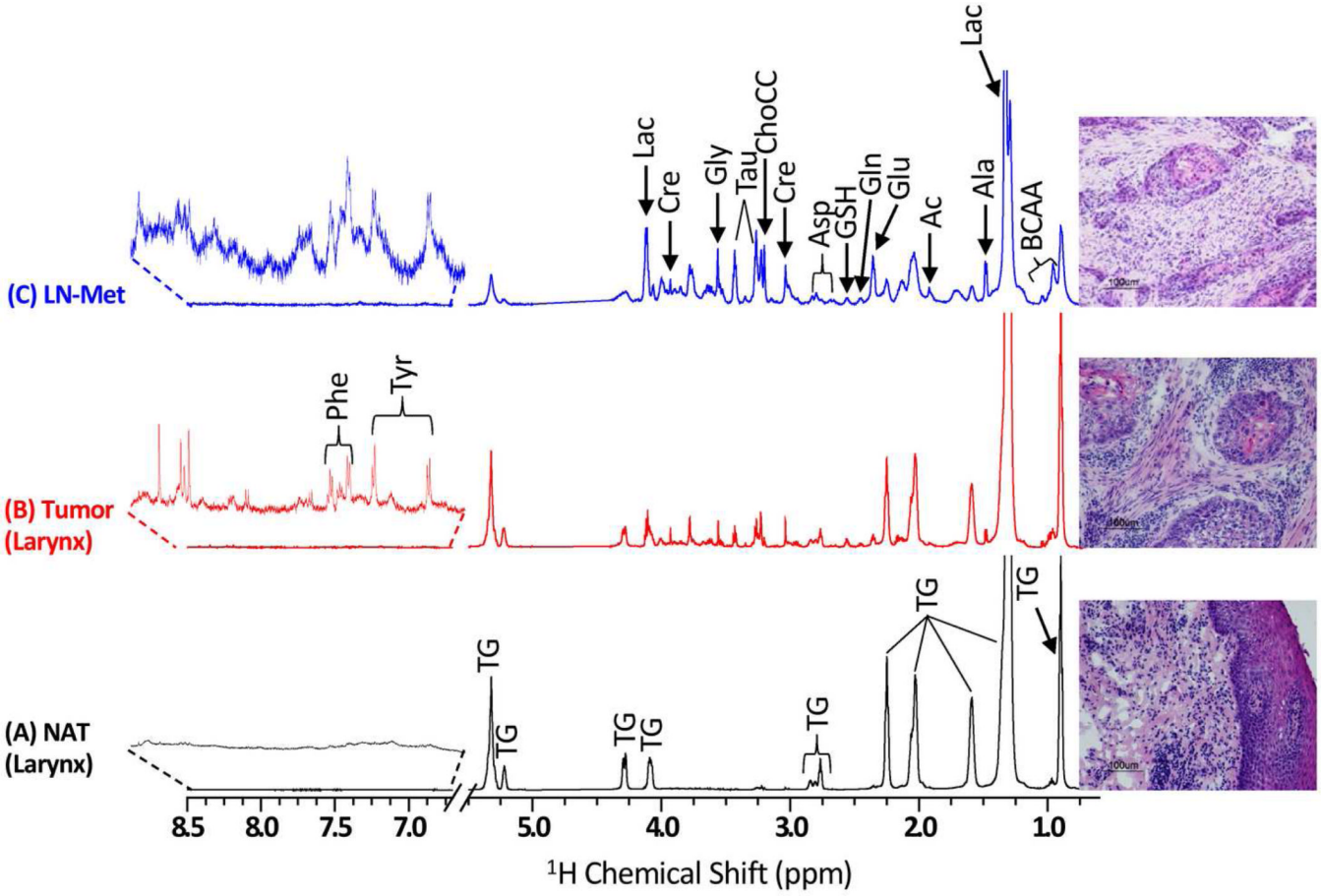

Figure 2.

Representative 600 MHz ^{1}H CPMG NMR spectra (area normalized) of (A) NAT, (B) Tumor and (C) LN-Met tissues taken from a single patient. The intensity of peaks in the chemical shift region 6.7 – 8.5 ppm was increased equally in all spectra to show the low-abundant taurine and phenylalanine. The corresponding H&E photomicrographs of post HR-MAS NMR tissues are shown alongside of each ^{1}H CPMG spectrum.

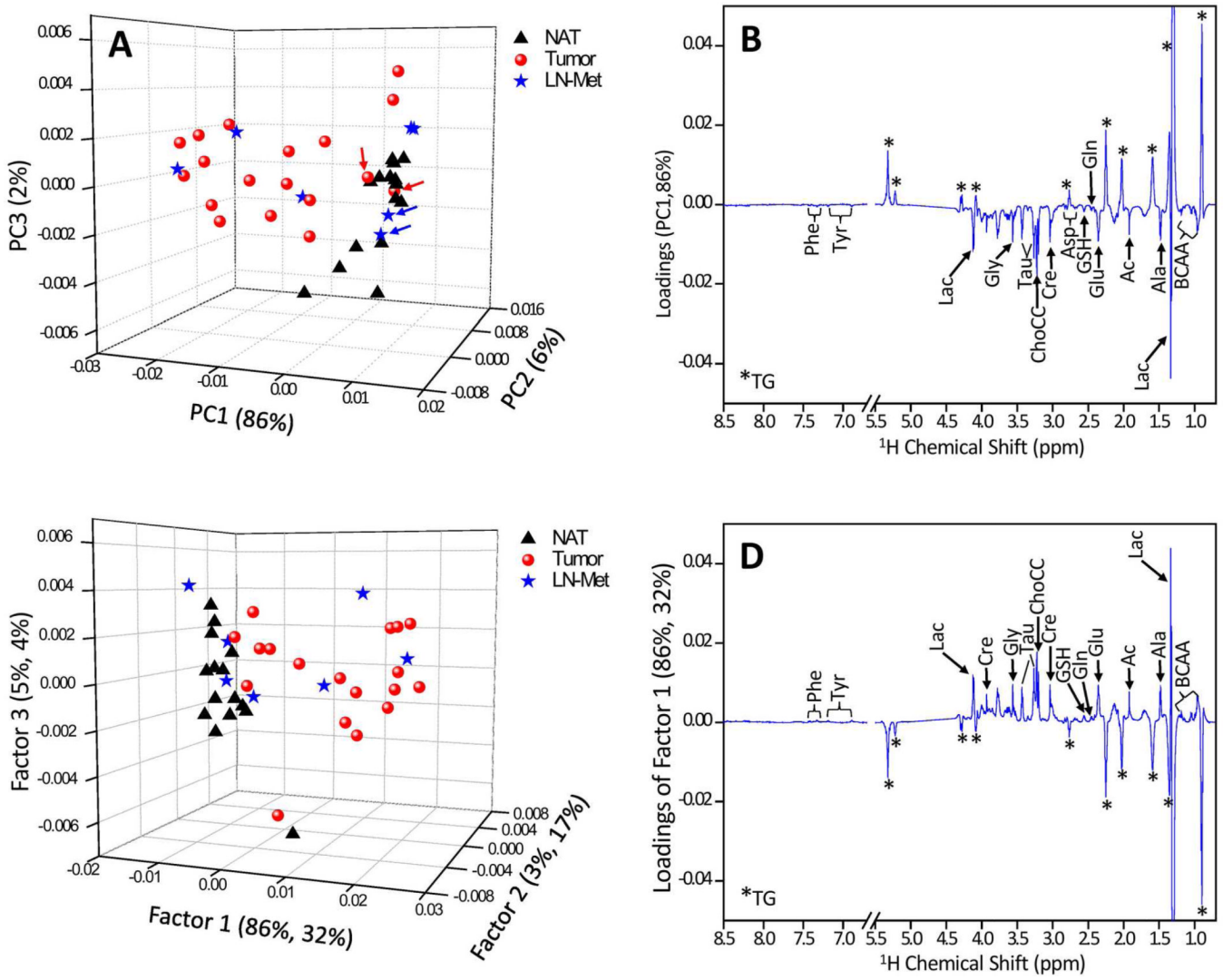

Figure 3.

(A) Unsupervised PCA and the corresponding (B) PC1 loadings, (C) PLS-DA and the corresponding (D) PC1 loadings of a total of 40 tissues generated from 15 NAT, 18 Tumor and 7 LN-Met tissues. It can be seen that primarily PC1 was responsible for the separation between NAT and tumor tissues; however, LN-Met tissues overlap with tumors. In PCA score plot, the tumor and metastatic tissues which were overlapping with that of NAT (indicated by red and blue arrows) are diagnosed as poorly differentiated squamous cell carcinoma. In the case of PLS-DA score plot (B), LN-Met tissues are indicated in different colors despite the analysis was carried out by considering LN-Met tissues as tumor.

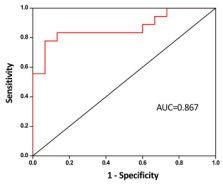

Figure 4.
ROC generated from predicted Y-values of PLS-DA. AUC of 0.876 represents a good predictability of PLS-DA model in differentiating NAT and tumor tissues.

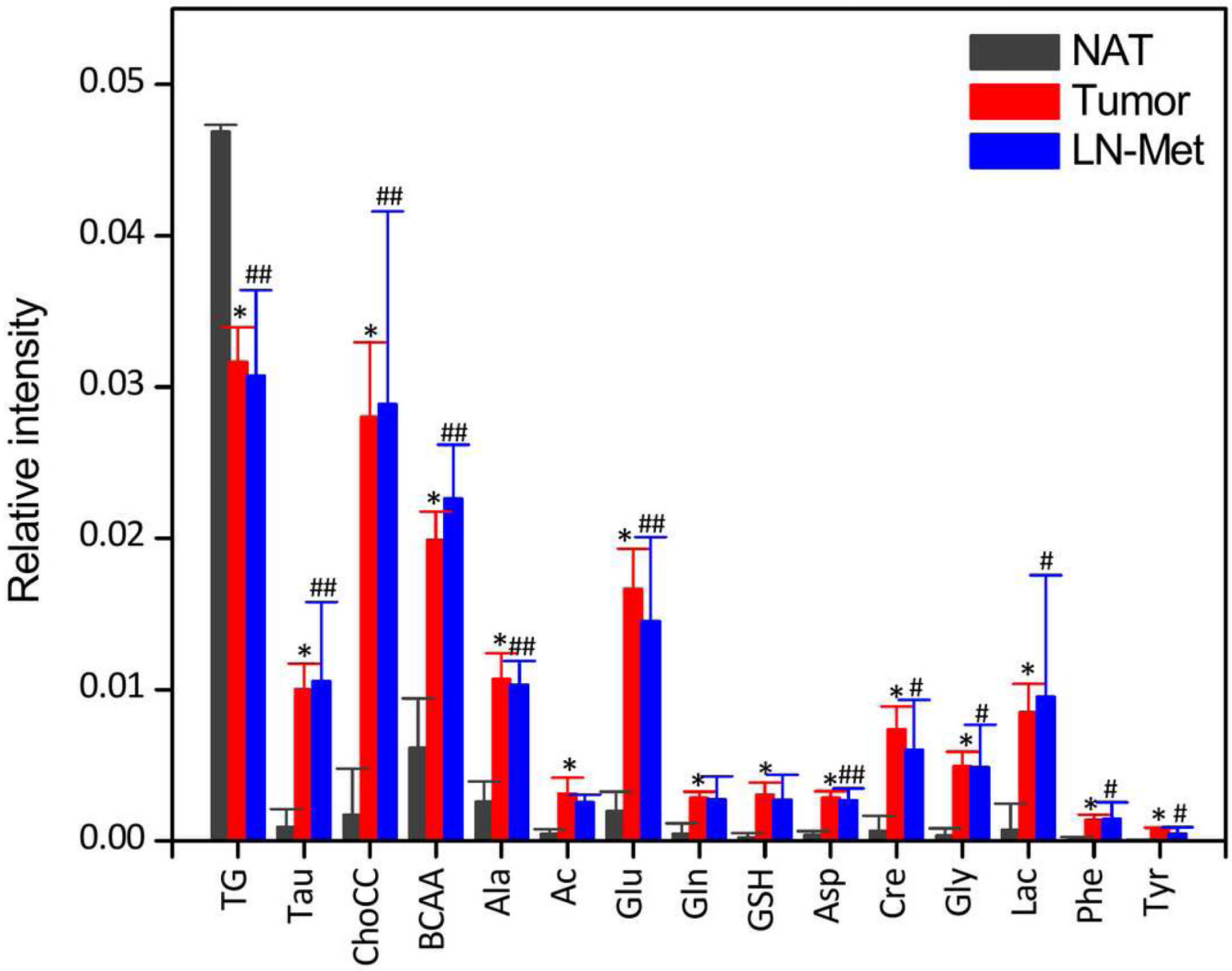

Figure 5.

Relative intensities (mean ± SEM) of triglycerides and metabolites obtained from normalized CPMG NMR spectra along with univariate statistical analysis (Mann-Whitney). * P < 0.001: NAT Vs Tumor; # P < 0.05: NAT Vs LN-Met; ## P < 0.01: NAT Vs LN-Met. There is no significant difference in the level of metabolites identified from tumor and LN-Met samples.

Table 1

Clinical characteristics of HNSCC patients

Patient No	Sex/Age	Specimen type	Diagnosis	Grade	TNM	Stage
1	M/58	Tongue	NAT/Tumor	G2	$T_1N_0M_0$	I
2	M/62	Tongue	NAT/Tumor	G2	$T_3N_0M_0$	III
3	F/64	Tongue	NAT/Tumor	G3	$T_{4a}N_{2b}M_0$	IVA
4	M/79	Tongue	NAT/Tumor	G3	$T_3N_0M_0$	III
5	F/72	Oral cavity	NAT/Tumor	G2	$T_2N_0M_0$	II
6	F/39	Oral cavity	NAT/Tumor	G2	$T_3N_1M_0$	IVA
7	M/57	Oral cavity	NAT/Tumor	G1	$T_4N_0M_0$	IVA
8	F/88	Lip	NAT/Tumor	G2	$T_3N_0M_0$	III
9	F/83	Lip	NAT/Tumor	G3	$T_3N_0M_0$	III
10	M/59	Larynx	NAT/Tumor	G2	$T_3N_0M_0$	III
11	M/50	Larynx	NAT/Tumor	G3	$T_3N_0M_0$	III
12	M/70	Larynx	NAT/Tumor	G2	$T_3N_0M_0$	III
13	M/59	Larynx	NAT/Tumor	G2	$T_3N_0M_0$	III
14	M/67	Larynx	NAT/Tumor	G1-G2	$T_1N_{2b}M_0$	IVA
15	M/67	Larynx	NAT/Tumor	G2	$T_3N_1M_0$	III
16	M/63	Larynx	NAT/Tumor	G2	$T_{4a}N_1M_0$	IVA
		Lymph Node	Metastases			
17	M/57	Larynx	NAT/Tumor	G2	$T_2N_{2b}M_0$	IVA
		Lymph Node	Metastases			
18	M/53	Larynx	NAT/Tumor	G2	$T_2N_{2b}M_0$	IVA
		Lymph Node	Metastases			
19	M/59	Lymph Node	Metastases	G2	$T_3N_1M_0$	III
20	M/48	Lymph Node	Metastases	G1	$T_2N_1M_0$	III
21	M/58	Lymph Node	Metastases	N/A	Recurrent	N/A
22	F/61	Lymph Node	Metastases	G1	$T_2N_{2b}M_0$	IVA